

## REPORT 1310

# AN INVESTIGATION OF FOUR WINGS OF SQUARE PLAN FORM AT A MACH NUMBER OF 6.9 IN THE LANGLEY 11-INCH HYPERSONIC TUNNEL<sup>1</sup>

By CHARLES H. McLELLAN, MITCHEL H. BERTRAM, and JOHN A. MOORE

### SUMMARY

The results of pressure-distribution and force tests of four wings at a Mach number of about 6.9 and a Reynolds number of  $0.98 \times 10^6$  in the Langley 11-inch hypersonic tunnel are presented. The wings had a square plan form, a 5-percent-chord maximum thickness, and diamond, half-diamond, wedge, and half-circular-arc sections.

Large deviations of the measured pressures from those predicted by the inviscid-flow theory were found at the leading edge of the wings and just behind sudden changes in surface slope. These pressure deviations were attributed to a rapid growth of the laminar boundary layer at the high test Mach number. The effect of boundary layer on the pressures on a flat surface parallel to the free stream was in good agreement with results of a theoretical investigation in which the boundary layer was assumed to be laminar. Separation effects similar to those normally encountered at lower Mach numbers were also present at the rear of the airfoils.

The effects of the departures of the pressures from those predicted by inviscid-flow theory over the various parts of the airfoils tended to compensate each other; thus the wing aerodynamic characteristics due to pressure forces can be predicted with reasonable accuracy by two-dimensional inviscid-flow theory at a Mach number of 6.9. At high angles of attack the experimental lift and drag results from force measurements were somewhat lower than the values given by the inviscid-flow theory because of separation and tip effects. At low angles of attack, the skin friction must be taken into account in calculating the total drag coefficients and lift-drag ratios of wings.

The two wings with symmetrical airfoil sections (the diamond and wedge sections) had the highest maximum lift-drag ratios as determined from pressure measurements and the half-circular-arc section had the lowest. The differences, however, were small when skin friction was included, the overall maximum lift-drag ratio being close to 6 for all the wings tested.

### INTRODUCTION

In evaluating the performance of contemplated high-speed air-sustained vehicles it is necessary to verify experimentally the predictions of theory. With the completion of flow surveys in a Mach number 6.9 nozzle in the Langley 11-inch hypersonic tunnel in 1949, the opportunity was presented for

a comparison of theory with experiment for some simple shapes at hypersonic speeds.

The results of an investigation made during 1949 and 1950 of the aerodynamic characteristics of four wings of square plan form at a Mach number of about 6.86 and a Reynolds number of  $0.98 \times 10^6$  based on the 4-inch wing chord are presented in this report. These wings were 5 percent thick and had diamond, half-diamond, half-circular-arc, and wedge airfoil sections. The wings with the diamond and wedge airfoil sections were tested through a range of angle of attack from  $0^\circ$  to about  $25^\circ$ , while the wings with the half-diamond and half-circular-arc airfoil sections were tested through a range from about  $-25^\circ$  to  $25^\circ$ . Both pressure and force measurements were made and compared with theoretical results.

### SYMBOLS

$b$	span
$C_D$	wing drag coefficient
$C_L$	wing lift coefficient
$c_n$	section normal-force coefficient
$x_{cp}$	distance from leading edge to center of pressure, chord lengths
$D$	drag
$L$	lift
$M$	free-stream Mach number
$p_\infty$	free-stream static pressure
$p_s$	surface static pressure
$p_b$	base pressure
$R$	Reynolds number based on free-stream conditions and wing chord
$x$	distance along chord, measured from leading edge
$y$	distance along span, measured from midspan
$\alpha$	angle of attack of airfoil or flat plate
Subscript:	
max	maximum

### DESCRIPTION OF APPARATUS AND MODELS

#### TUNNEL

The tests of this investigation were conducted in the Langley 11-inch hypersonic tunnel. This tunnel is of the blowdown type and has a test duration of 60 to 90 seconds, depending on the test configuration. A description of the

<sup>1</sup> Supersedes declassified NACA Research Memorandum L61D17 by Charles H. McLellan, Mitchel H. Bertram, and John A. Moore, 1951.

tunnel is given in reference 1. As shown in reference 2, the flow in the tunnel test section with the two-dimensional nozzle used during this investigation is sufficiently uniform for model testing in the 5-inch-square core of the stream. The Mach number in this region is about 6.86.

**MODELS**

The wings incorporated four airfoil sections—the diamond, half-diamond, wedge, and half-circular-arc (fig. 1). All the wings had a 4-inch chord, a thickness of 5 percent of the chord, and an aspect ratio of 1. Two sets of models were used, one designed for force measurements and the other for pressure measurements. The models, which were made of steel, were accurately machined and polished, and the surfaces and edges were maintained in good condition during the tests by periodic polishing. Special efforts were made to obtain sharp leading and trailing edges, and the thickness of these edges was between 0.001 and 0.002 inch. An additional model with a 20° wedge angle was included in order to obtain supplementary pressure data near the leading edge.

**MODEL SUPPORT SYSTEM**

The models were mounted on the support stings shown in figure 1. The stings were attached to a diamond-section support strut which spanned the tunnel vertically just downstream of the test section. (See refs. 1 and 2.) The pressure models were attached to their support stings by means of a swept offset arm affixed to the under surface of the models so that the upper surface, where the pressures were measured, was free from any obstruction. The angle of attack of the pressure models was varied by rotating the offset arm to predetermined settings.

The force models were attached to their support stings by a cone with 6.7° included angle. The 0.5-inch-diameter base of the sting was about 1.5 inches downstream of the trailing edge of the wing. The sting was affixed directly to the rear surface of the model with the cone axis parallel to the wing chord line. (See fig. 1.) The cone for the wedge model was attached to the blunt trailing edge. With the three-component force balance, the angle of attack was varied by using bent attachments to the sting. The bent sting attachments were shielded from the airstream. The angle of attack for

the two-component balance was varied by rotating the forepart of the sting that housed the balance.

**INSTRUMENTATION OF PRESSURE MODELS**

Pressure orifices were located along the chord of the model at the center line, as shown in figure 1. On most models, it was difficult to install a pressure orifice any closer to the leading or trailing edge than about 4 to 6 percent of the chord because of the thinness of the model. The leading edge of the wedge airfoil was so thin that the most forward orifice location was limited to about 12.5 percent of the chord from the leading edge.

Additional chordwise rows of orifices were installed in the wing with the diamond airfoil section at stations 31, 62.4, and 80.4 percent semispan from the center line. Orifices were also installed in the base of the wing with the wedge airfoil section. These were installed at 14, 37.6, 53, 71, and 95.6 percent semispan from the center line and halfway between the upper and lower surfaces.

In order to obtain pressures near the leading edge of a flat surface parallel to the stream, the special model was used which had a leading-edge included angle of 20°. This relatively large angle allowed orifices to be installed within about 0.125 inch of the leading edge. The large angle on the under side is not believed to have had an important effect on the pressure on the upper side.

Because of the thinness of the model, it was impractical to conceal inside the model the tubing which connected the orifice to the measuring instrument. A tube with 0.040-inch inside diameter formed the pressure orifice on one side and projected through the opposite surface where it was joined to a tube of 0.060-inch inside diameter (0.090-inch outside diameter) as shown in figure 1. At the high Mach number used in this investigation, the presence of the tube on one surface did not affect the pressures on the opposite surface except perhaps slightly at the trailing edge and at the base of the wedge model.

The pressures were measured by means of the aneroid-type six-cell recording units described in reference 1, which convert the deflection of a diaphragm into a rotation of a small mirror reflecting a beam of light to a moving film; thereby a time history of the pressure is recorded.

**INSTRUMENTATION OF THE FORCE MODELS**

The forces acting on the force models were measured by means of two strain-gage balances which were also part of the sting support for the model. Nearly all the force tests were made by using the three-component balance shown in figure 2, which was designed to measure lift, drag, and pitching moment. Pitching moments, however, were unreliable because of uneven heating of the pitch beams and thus were not used.

The instrumentation of the strain gages on the balance was such that temperature changes did not affect the calibration, provided that the whole balance was at a nearly uniform temperature. In order to reduce the amount of heating during tests, the exterior of the balance shield was coated with a porcelain insulation. The lift and drag components of this balance were designed for maximum

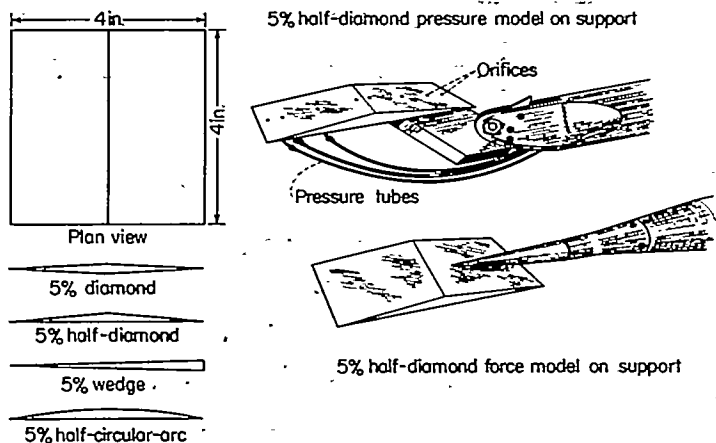


FIGURE 1.—Sketch of the airfoil models used to obtain aerodynamic characteristics at  $M=6.86$ .

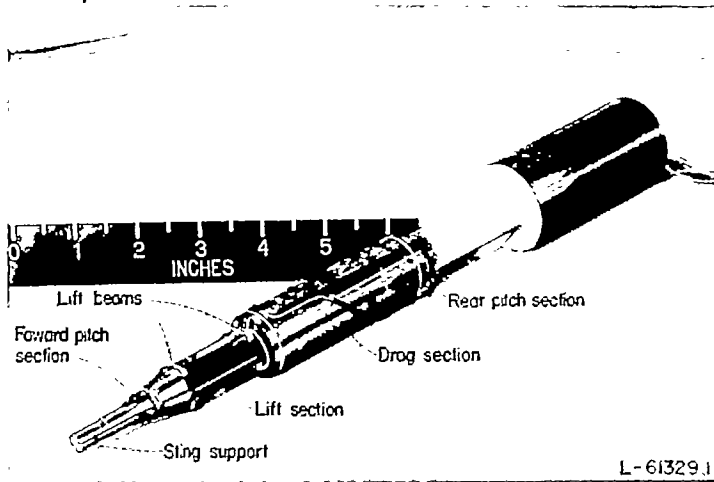


FIGURE 2.—Views of the disassembled three-component force balance.

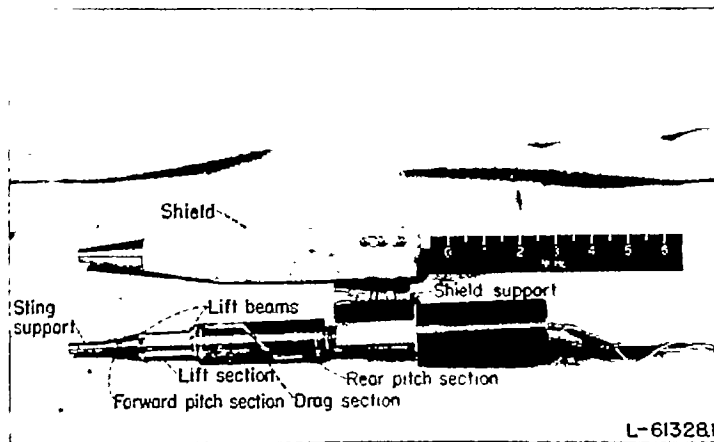


Figure 2.—Concluded.

measurable loads of 20 and 10 pounds, respectively, with an accuracy of 0.1 pound in lift and 0.05 pound in drag. In practice, this accuracy was not always realized because of uneven heating effects. These heating effects were somewhat erratic, at times being negligible and at other times having a moderate effect on the tare readings taken before and after the run.

A two-component strain-gage balance was designed to measure the lift and drag more accurately at low angles of attack than the three-component balance. This balance, which is shown in figure 3, was designed for a maximum normal load of 5 pounds and a maximum chordwise load of 1 pound; in each case, the balance was designed to give an accuracy of 1/2 percent of the maximum load. The effects of heating on this balance, however, were much greater in comparison with the design accuracy than the effects on the three-component balance, and therefore the relative accuracy was reduced somewhat.

**SCHLIEN SYSTEM**

The schlieren photographs presented in this report were taken by means of the schlieren system described in reference 1. Some of the photographs were taken with an exposure of 1/150 second and others with a flash of a few microseconds' duration. A horizontal knife-edge position was used for all photographs. The greatest limitation on

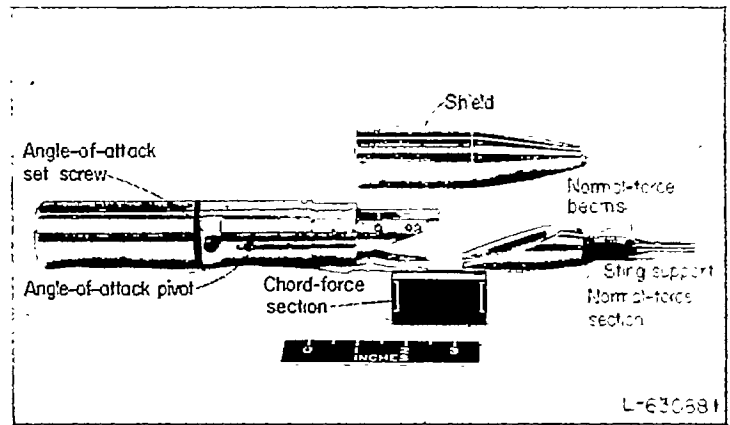


FIGURE 3.—View of the disassembled sensitive two-component force balance.

the sensitivity of this schlieren system is the heating effect on the windows. Since the stagnation temperature of the air in the tunnel was about 730° F for most tests, the inner surface of the glass windows became heated so that dark, nearly horizontal bands appeared in the schlieren photographs. In order to minimize this effect, most of the photographs used were obtained during the first part of the runs. The Mach number may, therefore, be as much as 3 percent lower than the calibrated value. The variation of Mach number with time is discussed in the following section.

**OPERATING CONDITIONS**

The tests were conducted at a stagnation pressure of approximately 25.5 atmospheres and a stagnation temperature of about 730° F. The high stagnation temperature is necessary to maintain the air temperature in the test section above the normal static liquefaction temperature. With the high stagnation temperature, a warpage of the first minimum of the nozzle takes place during the runs and results in a variation with time of about 3 percent in the test section Mach number. (See ref. 2.) By using only the test results obtained 60 seconds from the beginning of the runs, as was done in the nozzle calibration presented in reference 2, the effect of the varying Mach number was practically eliminated.

The Reynolds number for these tests was about  $0.98 \times 10^6$ , based on a 4-inch chord. This Reynolds number corresponds to a wing with a 4-foot chord flying at the test Mach number at an altitude of about 124,000 feet or a 2-foot chord at an altitude of about 108,000 feet.

**DATA ACCURACY**

**TUNNEL FLOW CHARACTERISTICS**

The test section of the single-step nozzle used in this investigation had a central core of reasonably uniform flow about 5 inches square in cross section. The Mach number variation of the flow in the part of the core in which the wings were tested ranged from about 0.7 percent above to 0.2 percent below the mean Mach number of 6.86. The flow at the center of the test region was essentially parallel to the tunnel axis, whereas at the extremes of the test region the flow deviated about one-fourth degree in the vertical plane away from the horizontal plane passing through the

center line of the nozzle. In the horizontal planes in the test region, the deviation of the flow was negligible.

ANGLE OF ATTACK

The differences between the support systems used for the pressure tests and for the force tests necessitated two different methods of measuring angle of attack. For the pressure tests, the use of a rigid model support and lack of any significant deflections under any test conditions simplified angle-of-attack measurements. In this case, the angle of attack was determined before the test run by measuring the height of the leading and trailing edges of the model from the bottom surface of the nozzle which, at the test section, is a plane surface. The accuracy of measurement of the angle of attack by this method is within  $0.2^\circ$ .

The use of a relatively flexible support in tests of the force models made necessary the determination of the angle of attack during the test run. This angle was determined by measurements of the model angle with respect to the reference lines on the schlieren photographs. The accuracy of this method was also limited to about  $0.2^\circ$ .

PRESSURE MEASUREMENTS

The pressure cells used in this investigation have an accuracy of 0.5 percent of the full-scale reading. Full-scale deflection, however, was seldom attained. In the most sensitive of the pressure cells, the free-stream pressure was about one-fourth of the full-scale deflection; the accuracy in this case was about  $\pm 2$  percent.

In the calculation of the ratio  $(p_s - p_\infty)/p_\infty$  from pressures measured by the cells, the probable maximum error including the effect of possible error in angle-of-attack setting is about  $\pm 0.07$  when the ratio is zero, about  $\pm 2$  percent as the ratio approaches  $-1$ , and about  $\pm 3$  percent for very large ratios. The coefficients computed from these pressures have an accuracy of about  $\pm 0.003$  in lift and  $\pm 0.002$  in drag at low angles of attack while at the highest angles of attack tested the probable maximum error is  $\pm 0.008$  in lift and  $\pm 0.002$  in drag.

FORCE MEASUREMENTS

The errors in force coefficients arise mainly from errors in Mach number and static-pressure determination and from the force-balance sensitivity. Errors due to heating effects were reduced by discarding the results of tests in which excessive differences were noted between the tare readings before and after the test. The force measurements on the force models included the force due to the conical support and its interference effects. Corrections were applied to the lift and drag results of the wing force tests to account for the aerodynamic forces on the unshielded portion of the conical support. These corrections were based on theoretical results for complete cones and limited experimental checks. No attempt was made to determine the effects of interference, but these are believed to be small because the area affected by the shocks from the support constitutes less than 5 percent of the wing surface area.

At low angles of attack, the sensitivity of the balance was the predominant factor. For this condition, the probable

maximum errors in lift and drag coefficients were about  $\pm 0.003$  and  $\pm 0.0015$ , respectively. At high angles of attack, the accuracy of Mach number and static pressure measurement were the important factors. At the highest test angle, the probable maximum errors in lift and drag coefficients were about  $\pm 0.008$  and  $\pm 0.004$ , respectively.

PRESENTATION OF RESULTS

PRESSURE MEASUREMENTS

**Chordwise pressure distribution.**—The pressures over the midspan section of the wings at various angles of attack are presented in figures 4 to 8. The pressures measured at each orifice are presented as the nondimensional pressure rise  $(p_s - p_\infty)/p_\infty$ , where  $p_s$  is the local static pressure and  $p_\infty$  is the free-stream static pressure. This ratio has a value of zero when the local surface pressure is equal to the stream static pressure and has a value of  $-1$  when the absolute pressure on the surface is zero.

Theoretical two-dimensional pressure distributions over the models are also presented in figures 4 to 8. These distributions have been calculated by using the Prandtl-Meyer expansion equations and the oblique-shock relations. For the diamond, half-diamond, and wedge airfoil sections, this method gives exactly the same results as the shock and characteristics theory. For the half-circular-arc airfoil at the test Mach number, the differences in pressure distributions calculated from the Prandtl-Meyer equations and from the characteristics theory with rotational flow are negligible.

In order to simplify the presentation of the results, the pressures on the flat surface of the half-circular-arc wings have not been included; however, the tests gave the same results for the flat sides of the half-diamond and the half-circular-arc wings.

The results of a study of the pressure distribution over a flat surface parallel to the stream are presented in figure 9. The experimental pressures were obtained from the flat surfaces of several of the models and from the model with a  $20^\circ$  wedge angle.

The theoretical pressure distribution plotted in figure 9 is based on the assumption that, in effect, the boundary layer changes the shape of the body by an amount equal to the displacement thickness of the boundary layer. In calculating the boundary layer, laminar flow with a linear velocity profile and a Prandtl number of 1 along an insulated flat plate is assumed, and Sutherland's formula is used for the viscosity variation. A nearly linear distribution of velocity within the boundary layer at high free-stream Mach numbers was predicted from theoretical considerations in references 3 and 4. The variation of the theoretical pressure with distance along the chord (fig. 9), however, is not very sensitive to the shape of the boundary-layer profile and considerable variation in the velocity profile could, therefore, be tolerated without changing the theoretical results significantly.

A schlieren photograph showing the thick boundary layer over one of the wing models with one flat surface parallel to the stream is also included in figure 9, together with a schematic diagram of the model showing the boundary layer and upper-surface shock.

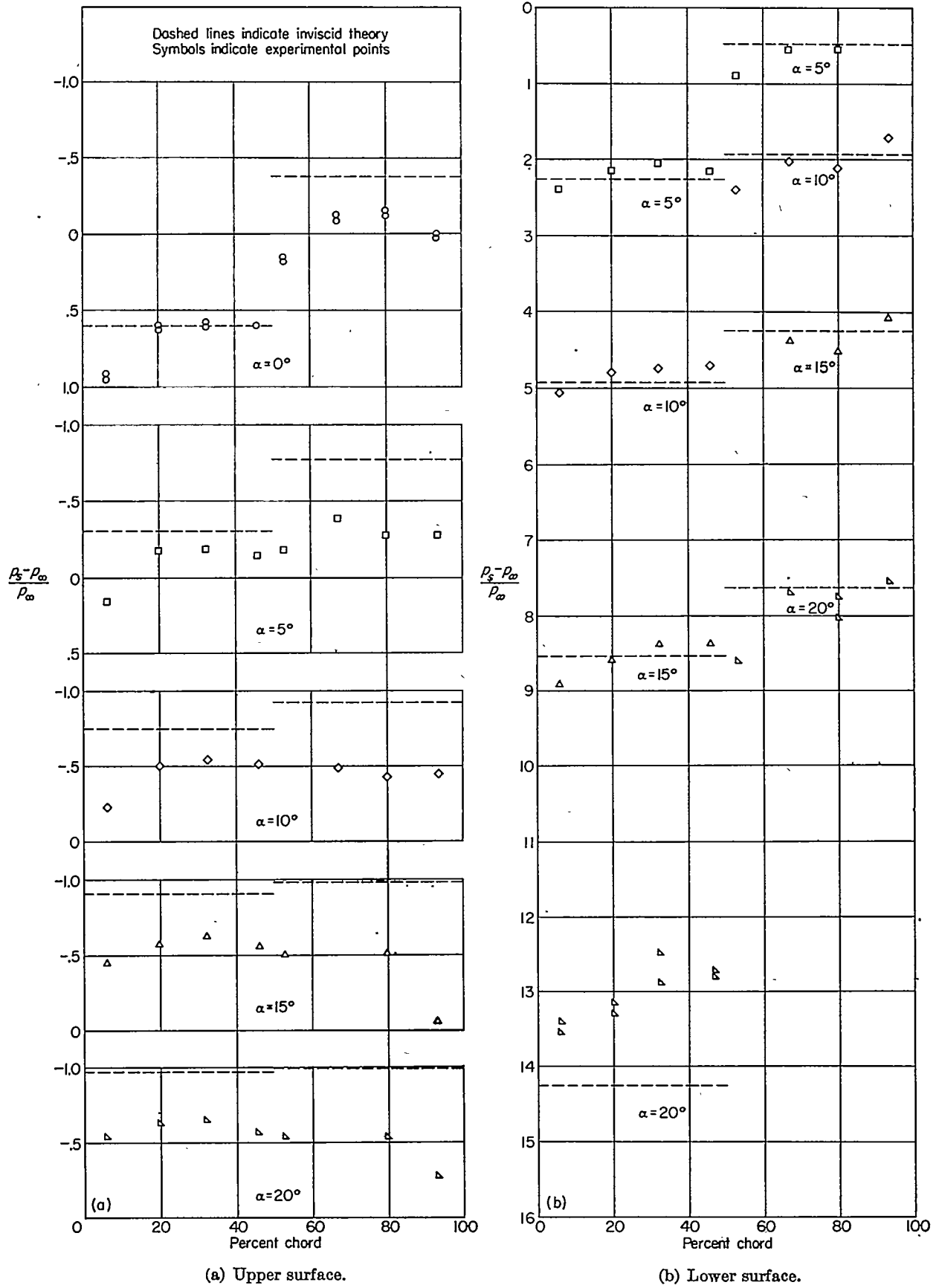


FIGURE 4.—Pressure variation over a 5-percent-thick diamond airfoil section at various positive angles of attack.  
 $M=6.86$ ;  $R=0.98 \times 10^6$ .

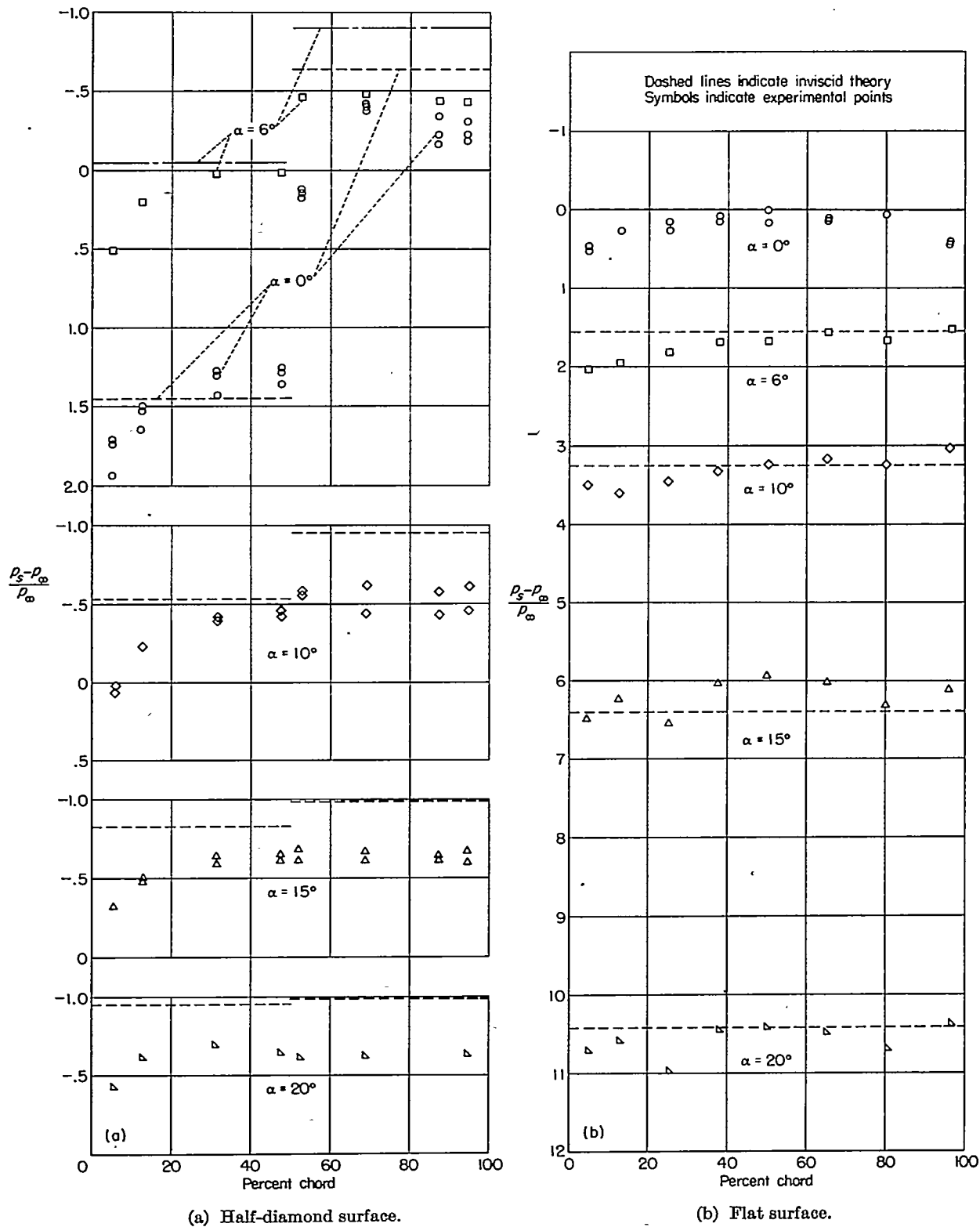
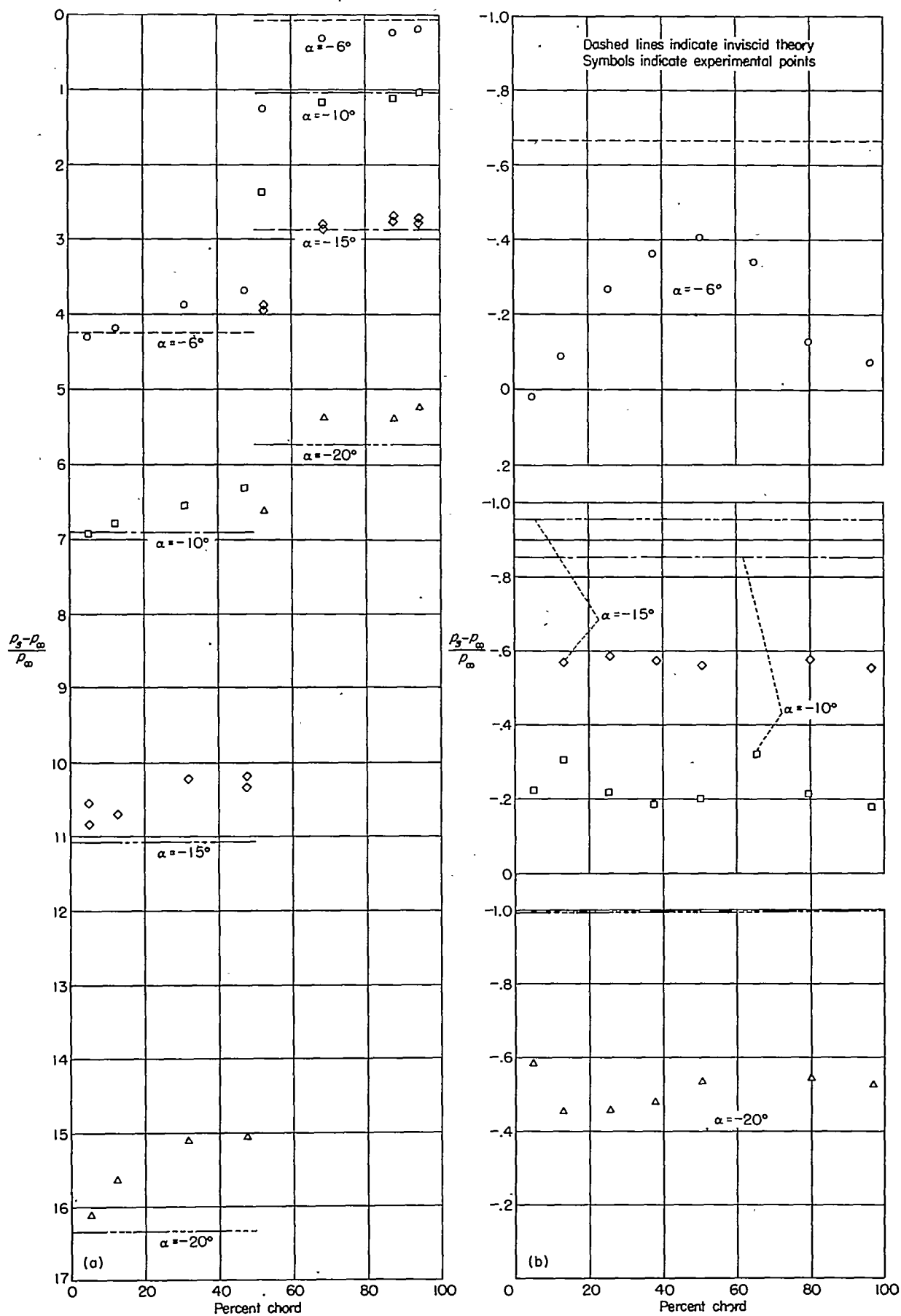


FIGURE 5.—Pressure variation over a 5-percent-thick half-diamond airfoil section at various positive angles of attack.  $M=6.86$ ;  $R=0.98 \times 10^6$ .



(a) Half-diamond surface. (b) Flat surface.  
 FIGURE 6.—Pressure variation over a 5-percent-thick half-diamond airfoil section at various negative angles of attack.  $M=6.86$ ;  $R=0.98 \times 10^6$ .

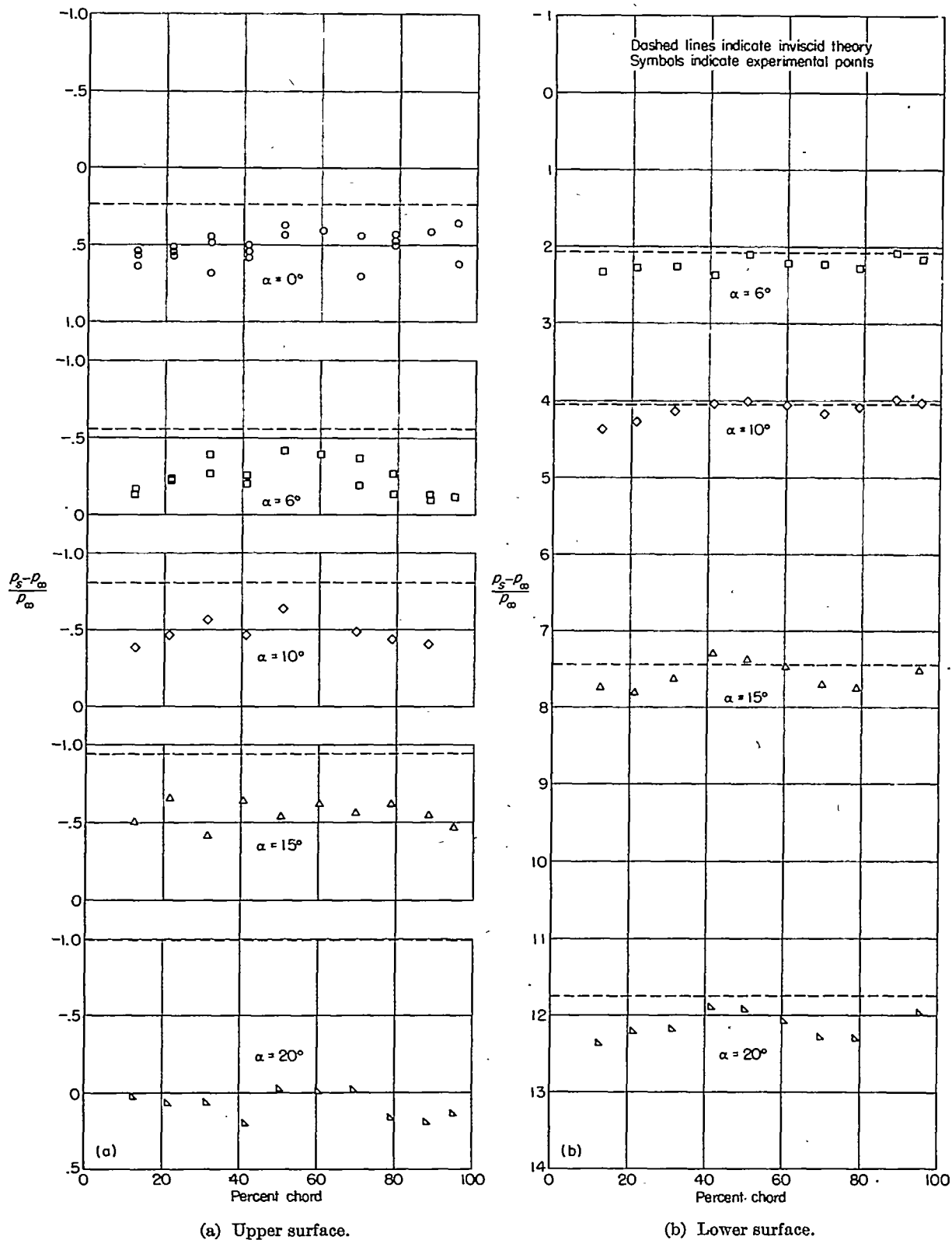


FIGURE 7.—Pressure variation over a 5-percent-thick wedge airfoil section at various positive angles of attack.  $M=6.86$ ;  $R=0.98 \times 10^6$ .



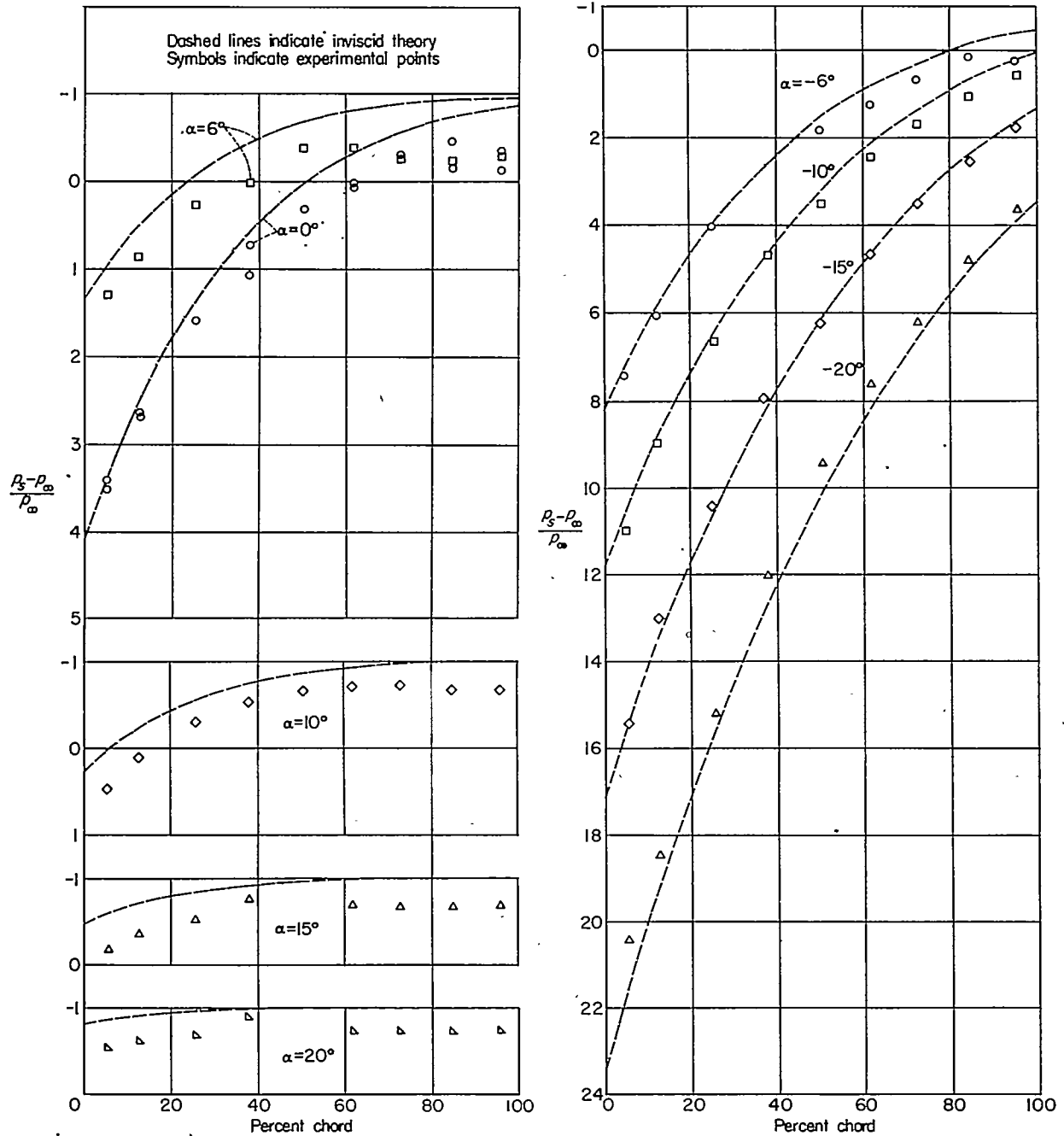


FIGURE 8.—Pressure variation over the upper surface of a 5-percent-thick half-circular-arc airfoil section at various angles of attack.  $M=6.86$ ;  $R=0.98 \times 10^6$ .

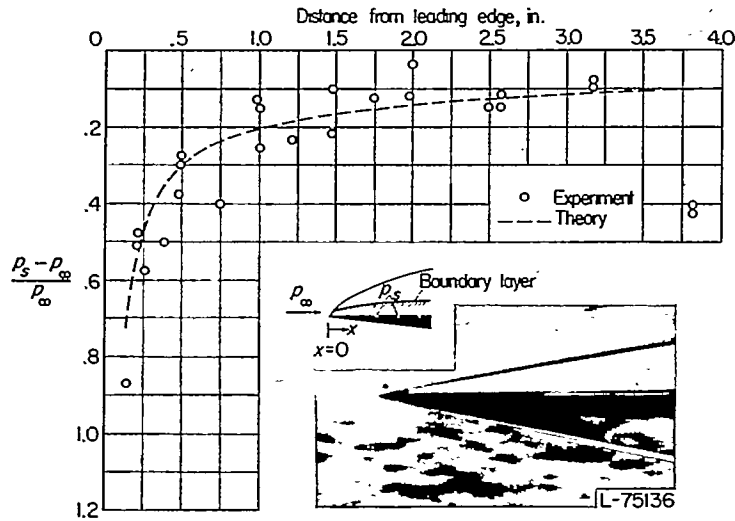


FIGURE 9.—Pressure distribution over a flat plate inclined at zero angle to an initial flow at  $M=6.86$  and  $R=0.98 \times 10^6$ .

Figure 10 presents the results of an investigation of the effect of the leading-edge thickness on the pressures at various distances from the leading edge of a flat surface parallel to the stream. These results were obtained by varying the leading-edge thickness of the  $20^\circ$  wedge from 0.001 to 0.008 of an inch. The thickness was varied by cutting off the leading edge normal to the upper surface.

Spanwise variation of pressure distributions and normal-force coefficients.—The chordwise pressure distributions at the four spanwise stations on the diamond airfoil are presented in figure 11 for an angle of attack of  $10^\circ$ . The theoretical pressure distributions are those given by the two-dimensional inviscid-flow theory and are shown only for the portions of the surface that are theoretically two-dimensional. Both the experimental and theoretical pressure distributions have been integrated to obtain the section normal-force coefficients which are presented in figure 12. The two-dimensional theoretical coefficients are included only as far outboard as the flow is theoretically two-dimensional over the whole chord. In order to show the individual

contributions of the upper and lower surfaces to the overall section lift coefficients, these surfaces are shown separately.

Base pressure on the wedge airfoil.—Base-pressure measurements were made on the wedge-section wing in order to complete the determination of the section characteristics of this wing. Base pressures were measured at five spanwise locations to avoid interference effects due to the support strut. The variation of base pressure with angle of attack is presented in figure 13.

WING CHARACTERISTICS

Figures 14 to 21 present the aerodynamic characteristics ( $C_L$ ,  $C_D$ ,  $x_{cp}$ , and  $L/D$ ) of the four wings. Results of both pressure measurements and force measurements are included. The coefficients obtained from pressures actually represent the section coefficients at the center of span and can be considered to represent the overall coefficients only if the tip effects are neglected. The coefficients from the force tests, on the other hand, include the tip effect and are actually overall coefficients of the wing.

The solid-line curves in figures 14 to 21 represent the two-dimensional theoretical coefficients obtained by integration of the theoretical inviscid pressure distributions. A calculated skin friction has been added to the drag coefficients and the results are presented as dashed-line curves. The drag coefficients including viscous effects have been calculated by making the same assumptions as were made for the calculation of the effect of the boundary layer on the pressure distribution over a flat plate parallel to the free stream. The friction drag coefficients for the diamond, half-diamond, wedge, and half-circular-arc wings at zero angle of attack were calculated to be 0.0028, 0.0030, 0.0029, and 0.0029, respectively. These values of the friction coefficients were corrected for a slight variation with angle of attack.

The theoretical curves in figure 18 are for a base pressure on the wedge airfoil equal to one-half of the stream pressure, which is roughly the value obtained from pressure measurements. No attempt was made to evaluate the base pressure theoretically. The variation in the coefficients due to changing the base pressure by an amount equal to one-half of the stream pressure in either direction would be very small and not noticeable in this figure. This variation in base pressure, however, has an appreciable effect on the lift-drag ratios for the wedge airfoil, which are presented in figure 19. In this figure, the theoretical lift-drag ratios are presented for three values of base pressure even though the base pressures measured were approximately one-half of free-stream pressure.

SCHLIEREN PHOTOGRAPHS

Typical schlieren photographs of the flow about the wing with the diamond airfoil section are presented in figure 22. As these photographs were taken with the model mounted on the force balance, the trailing edge of the model is hidden by the sting mounting. The location of the trailing edge can be estimated by noting the surface discontinuity (at the maximum thickness) which occurs at the 50-percent-chord station.

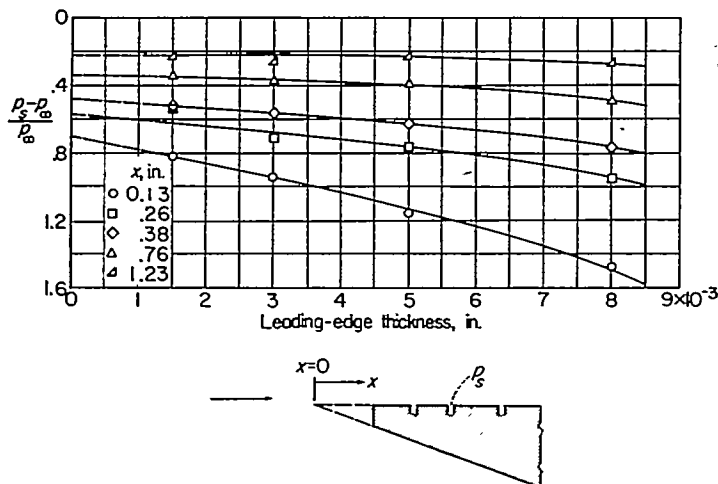


FIGURE 10.—Effect of leading-edge thickness on pressures over a flat plate inclined at zero angle to an initial flow at  $M=6.86$  and  $R=0.98 \times 10^6$ .

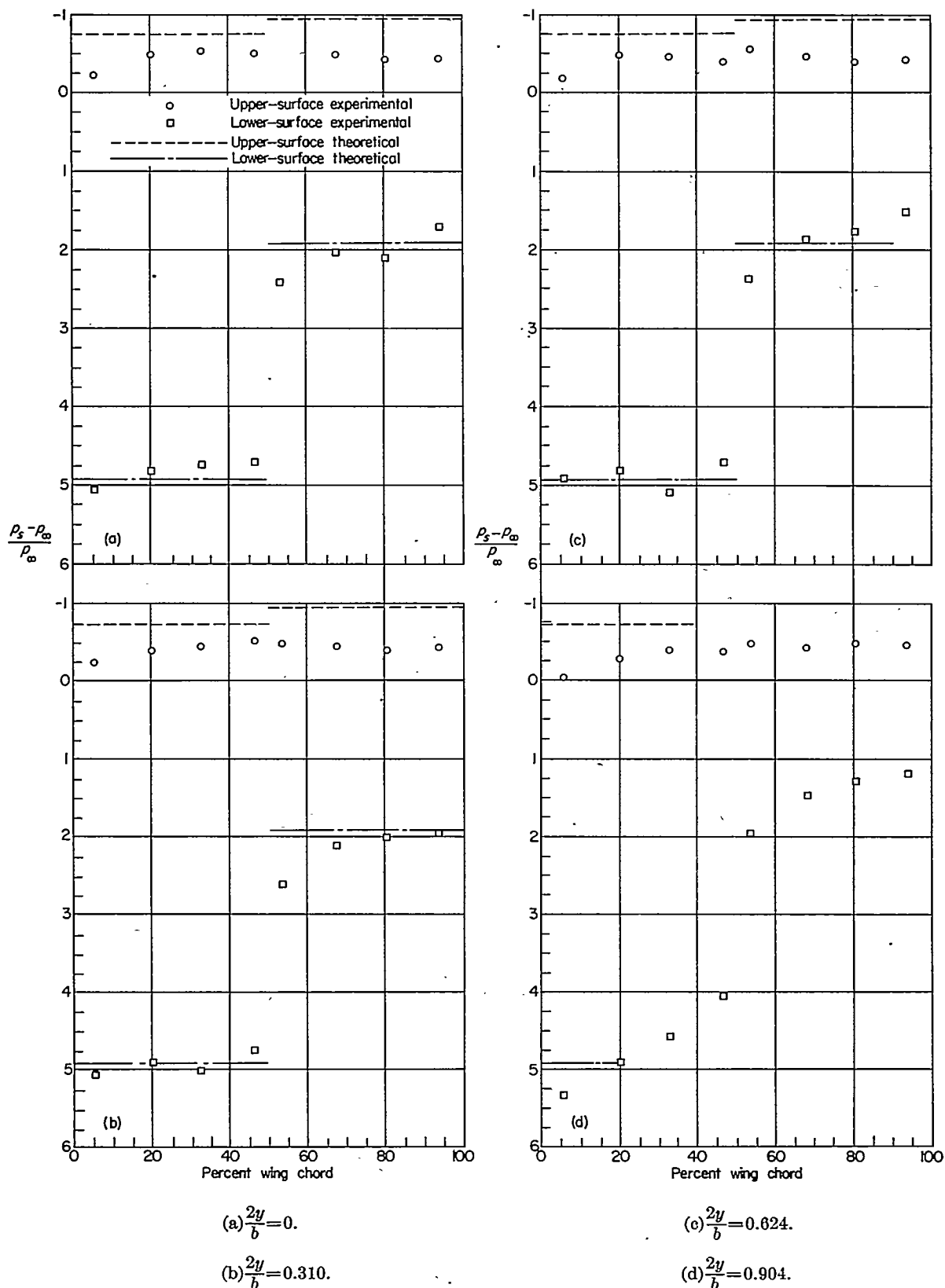


FIGURE 11.—Chordwise pressure distribution over a 5-percent-thick diamond-section airfoil at  $\alpha=10^\circ$  for various spanwise stations, measured from midspan.  $M=6.86$ ;  $R=0.98 \times 10^6$ .

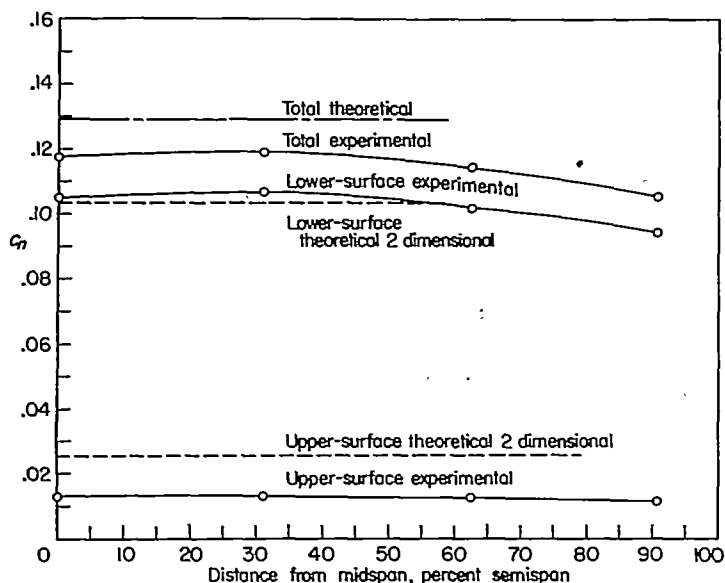


FIGURE 12.—Spanwise variation of section normal-force coefficient over the 5-percent-thick diamond-section airfoil at  $\alpha=10^\circ$ .  $M=6.86$ ;  $R=0.98 \times 10^6$ .

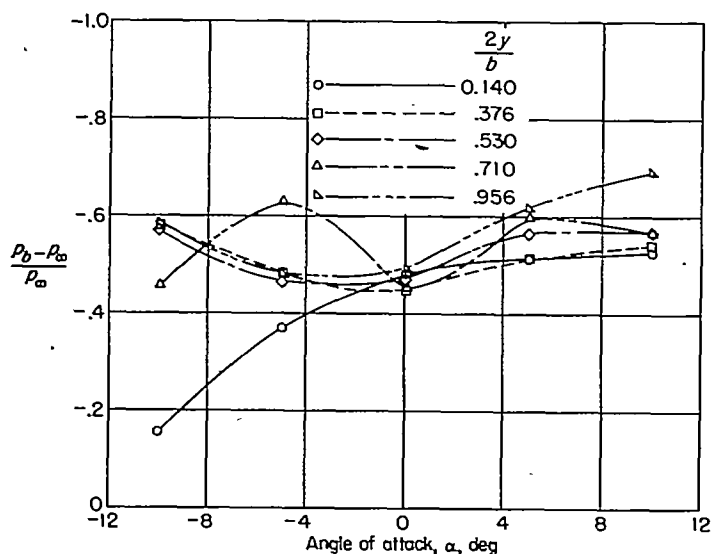


FIGURE 13.—Base pressures over the  $20^\circ$  wedge-airfoil pressure model as a function of angle of attack for various distances from midspan.  $M=6.86$ ;  $R=0.98 \times 10^6$ .

**DISCUSSION**  
**PRESSURE RESULTS**

The pressure data of figures 4 to 7 show large deviations from the pressures predicted by inviscid theory. In addition to the usual departures of the measured pressures from those predicted by theory for supersonic flow in the region near the trailing edge, which are attributed to separation caused by an interaction between the boundary layer and the trailing-edge shock, the pressures also show large rises at the leading edges and just rearward of abrupt changes in the slopes of model surfaces. (See, for example, figs. 4, 5, and 6.) These pressure rises at the leading edges are evident even for the case of a flat surface parallel to the flow, for which inviscid theory indicates no pressure rise.

The leading-edge pressure rise could conceivably be caused by either leading-edge thickness effects or by viscous effects, and both of these possibilities were investigated.

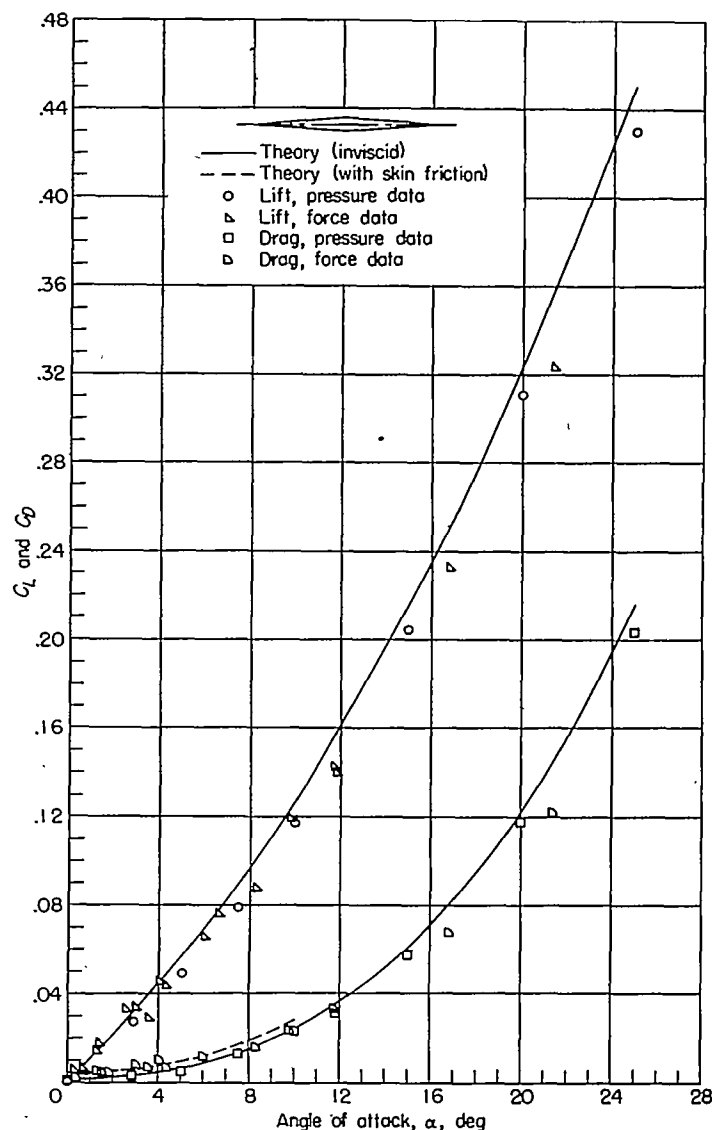


FIGURE 14.—Variation of lift and drag coefficients with angle of attack for a 5-percent-thick diamond-section airfoil.  $M=6.86$ ;  $R=0.98 \times 10^6$ .

**Effect of leading-edge thickness.**—In figure 10, pressure data obtained in tests of a wedge with the upper surface parallel to the flow show that at the most forward station on the wedge, 0.13 inch downstream of the leading edge, the pressure ratio  $(p_s - p_\infty)/p_\infty$  nearly doubles as the leading-edge thickness is increased from 0.0015 inch to 0.008 inch. Since the thickness of the leading edges of all models tested did not exceed 0.002 inch, the pressure rise due to leading-edge thickness is small and cannot be considered the major cause of the pressure rise at the leading edge of the wings tested.

**The boundary layer and its effect on the flow.**—An analysis was made to determine the rate of growth of the boundary layer on a flat plate at a Mach number of 6.86 for laminar flow and a linear velocity profile. At a Mach number of 7, the calculated boundary-layer displacement thickness is about 10 times as thick as at a Mach number of 1 for equivalent Reynolds numbers. Pressure distributions calculated for the flat surface with boundary layer are in good agreement with the experimental data (fig. 9). Interaction of the shock and boundary layer at the leading edge was neglected. This analysis has shown that the large pressure

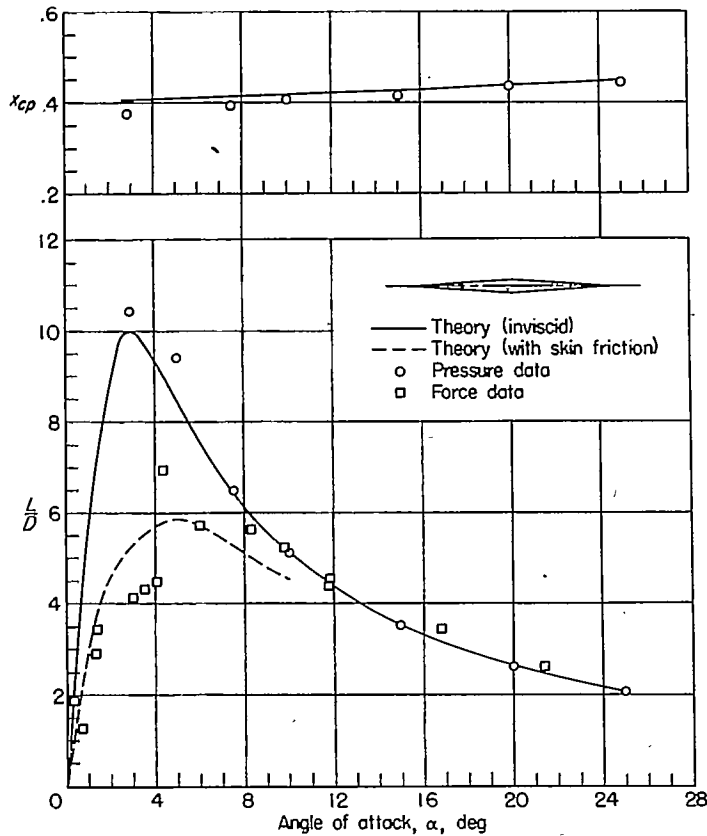


FIGURE 15.—Variation of the center of pressure and the lift-drag ratio with angle of attack for a 5-percent-thick diamond-section airfoil.  $M=6.86$ ;  $R=0.98 \times 10^6$ .

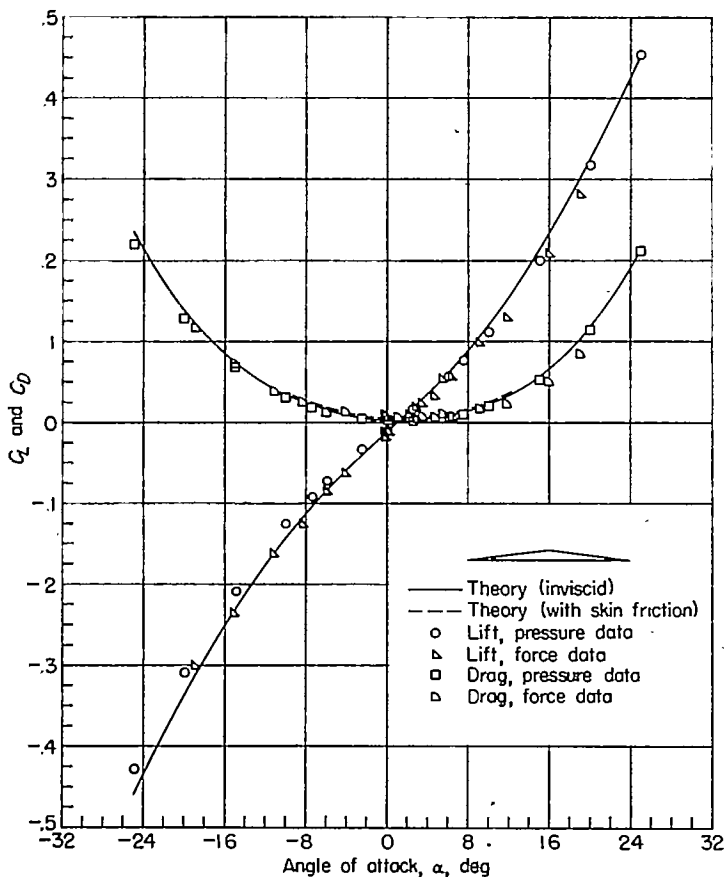


FIGURE 16.—Variation of lift and drag coefficients with angle of attack for a 5-percent-thick half-diamond-section airfoil.  $M=6.86$ ;  $R=0.98 \times 10^6$ .

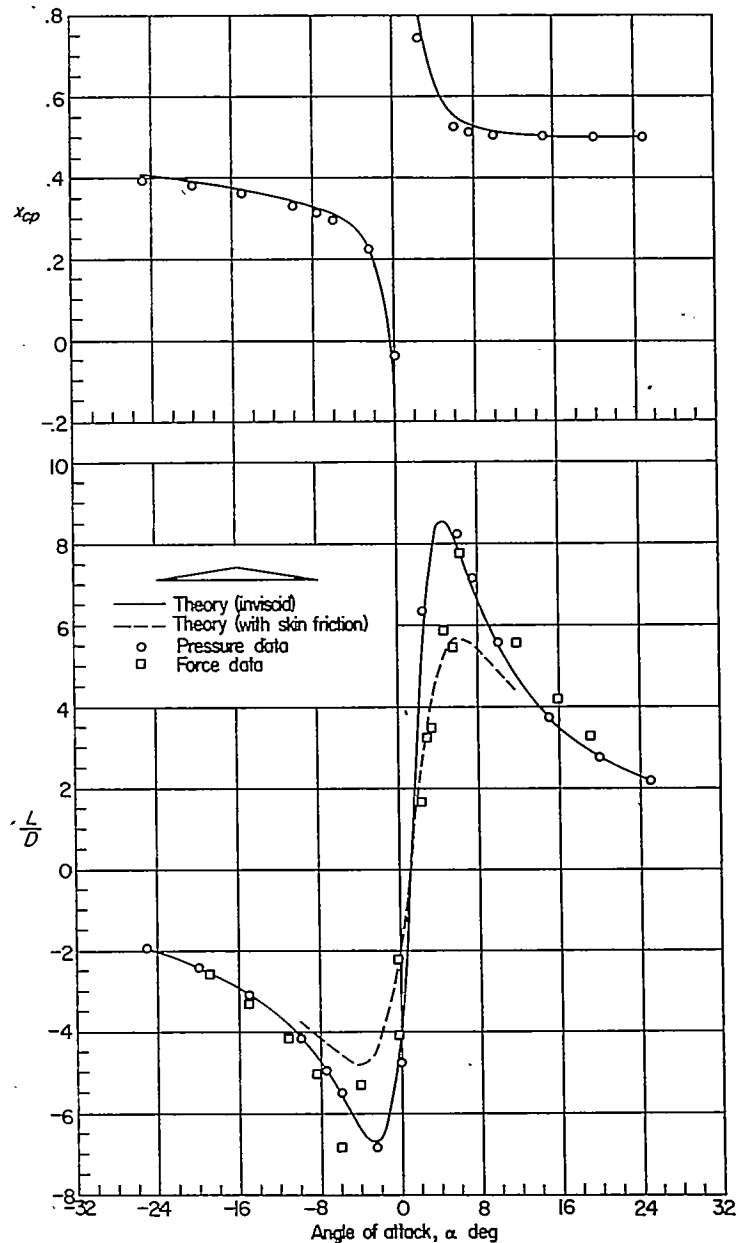


FIGURE 17.—Variation of center of pressure and lift-drag ratio with angle of attack for a 5-percent-thick half-diamond-section airfoil.  $M=6.86$ ;  $R=0.98 \times 10^6$ .

rise at the leading edge is primarily due to the very rapid growth of the boundary layers at high Mach numbers. A more complete analysis of the boundary-layer displacement effect and leading-edge-thickness effect is given in references 5 and 6.

Further experimental verification of the large thickness of the boundary layer was obtained by means of schlieren photographs. This thick boundary layer is apparent in the schlieren photograph in figure 9, which shows the flow about a wedge with the upper surface parallel to the air stream. Since the surface is parallel to the free stream, the presence of the shock is attributed to the boundary layer at the leading edge and the finite leading-edge thickness. Behind the leading edge the schlieren photograph shows the boundary layer as light and dark bands just above the model surface. The method of model support unfortunately prevented schlieren observation of the flow at the trailing edge.

Pressures greater than those predicted by theory also

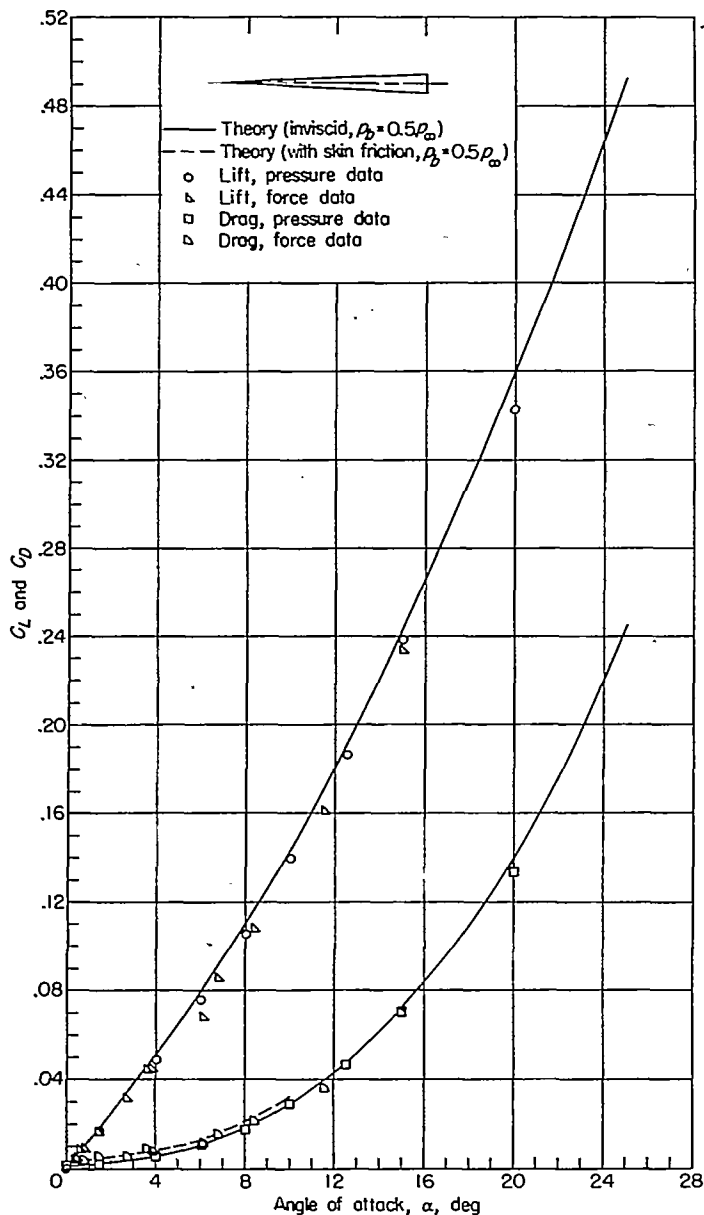


FIGURE 18.—Variation of lift and drag coefficients with angle of attack for a 5-percent-thick wedge-section airfoil.  $M=6.86$ ;  $R=0.98 \times 10^6$ .

occur just behind abrupt changes in the slope of the surface, such as the maximum thickness of the diamond airfoil (fig. 4). The effect of the change in direction of the surface is not felt by the stream outside the boundary layer for an appreciable distance behind the change in the surface slope. The schlieren photograph of the diamond airfoil at an angle of attack of  $0.5^\circ$  (fig. 22 (a)) indicates that the point at which the flow outside the boundary layer changes direction is a distance of about 5 percent chord downstream of the change in surface slope; in addition, the effect of the turning of the air outside the boundary layer cannot be felt at the surface for an appreciable distance downstream of the point where the outside flow is deflected. The overall effect of this lag is to smooth out over a greater area the abrupt pressure changes which would otherwise occur at the change in surface slope.

The effect of the boundary layer on the pressures on the curved surface of the half-circular-arc airfoil is somewhat

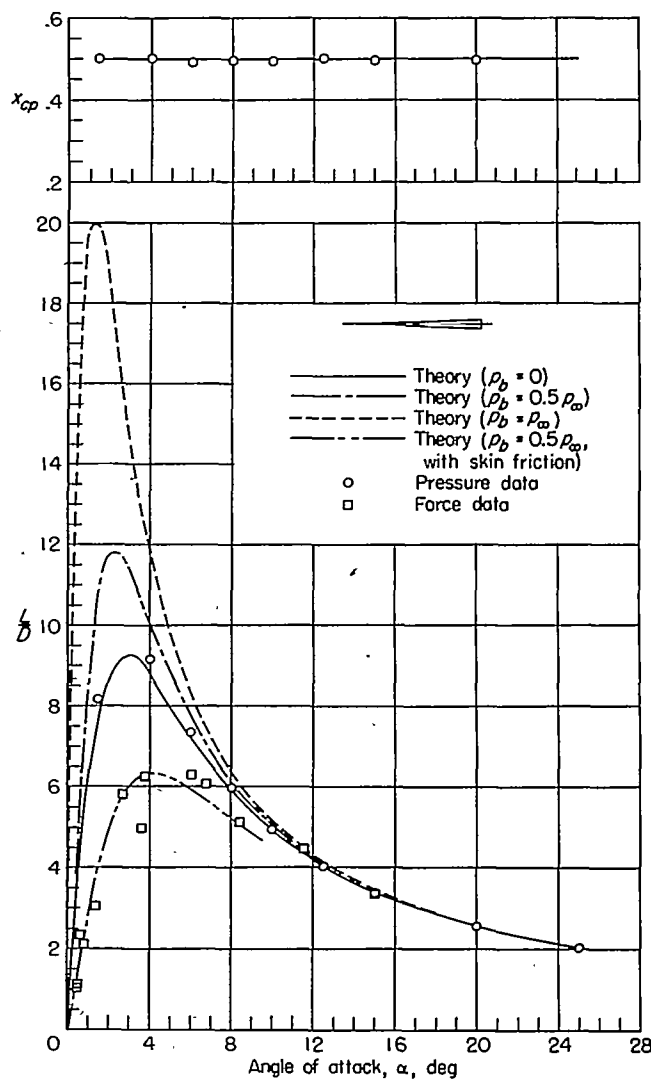


FIGURE 19.—Variation of center of pressure and lift-drag ratio with angle of attack for a 5-percent-thick wedge-section airfoil.  $M=6.86$ ;  $R=0.98 \times 10^6$ .

different from that for a flat plate. At low angles of attack, a strong shock occurs on the curved surface of the airfoil and is followed by a relatively low Mach number which increases with distance from the leading edge. At the reduced Mach numbers over the forepart of the surface, the rate of growth of the boundary layer is relatively slow. Farther back along the surface, where the Mach number is higher and the density therefore lower, the boundary layer thickens rapidly. The result of this increase in the rate of boundary-layer growth is an increase in the pressures over the entire curved surface, rather than primarily near the leading edge as in the case of the flat plate. (See ref. 5.)

Span-load distribution.—As shown by figure 12, over the upper surface the spanwise variation of the normal-force coefficient is nearly constant but the experimental values of section normal-force coefficient are only about one-half of the values predicted by theory for two-dimensional flow. The data of figure 11, together with those of figure 4, indicate that the flow is separated just behind the maximum thickness, a condition which is evident at all four spanwise stations. These pressure data show no appreciable effect of the tip over the upper surface even though at the wing attitude and

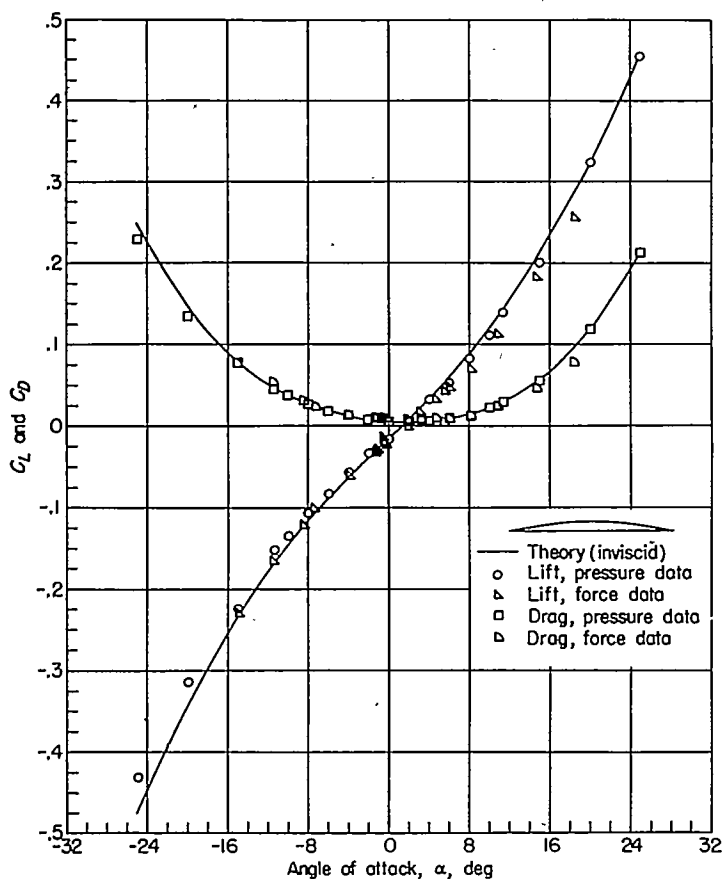


FIGURE 20.—Variation of lift and drag coefficients with angle of attack for a 5-percent-thick half-circular-arc-section airfoil.  $M=6.86$ ;  $R=0.98 \times 10^6$ .

Mach number of figure 11 the rear 60 percent of the upper surface at the outermost spanwise station ( $\frac{2y}{b}=0.904$ ) would be in a region of three-dimensional flow. Thus, the constancy of the normal force along the span on the upper surface is largely due to separated flow on the entire rear half of the wing.

The results from lower-surface pressures (fig. 12) show good agreement with theory in the region of two-dimensional flow but also indicate a gradual decrease in normal force as the tip is approached. The pressure data of figure 11 show that essentially two-dimensional flow exists over the two innermost spanwise stations and that the section normal force in this region of two-dimensional flow is in good agreement with theory. At the two outermost spanwise stations, however, three-dimensional flows exist. Calculations show that three-dimensional flow existed over the rear 10 percent of the wing at the  $\frac{2y}{b}=0.624$  station and over the rear 80 percent at the  $\frac{2y}{b}=0.904$  station.

Base pressures on the wedge airfoil section.—The plots of base pressure against angle of attack in figure 13 indicate that the interference near the midspan ( $\frac{2y}{b}=0.140$ ) was appreciable for negative angles of attack, with the model supported from the under side. The curves would be symmetrical about an angle of attack of zero if no interference effects were present. Except for the station nearest the midspan,

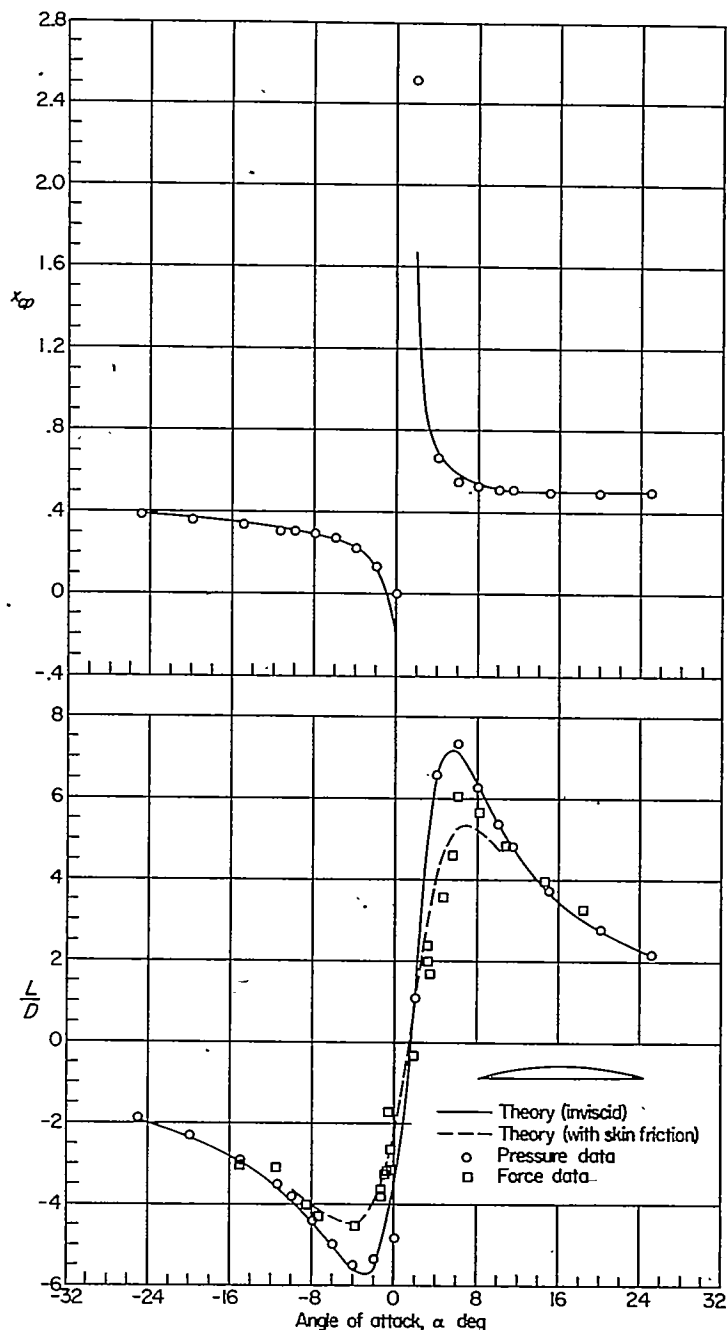
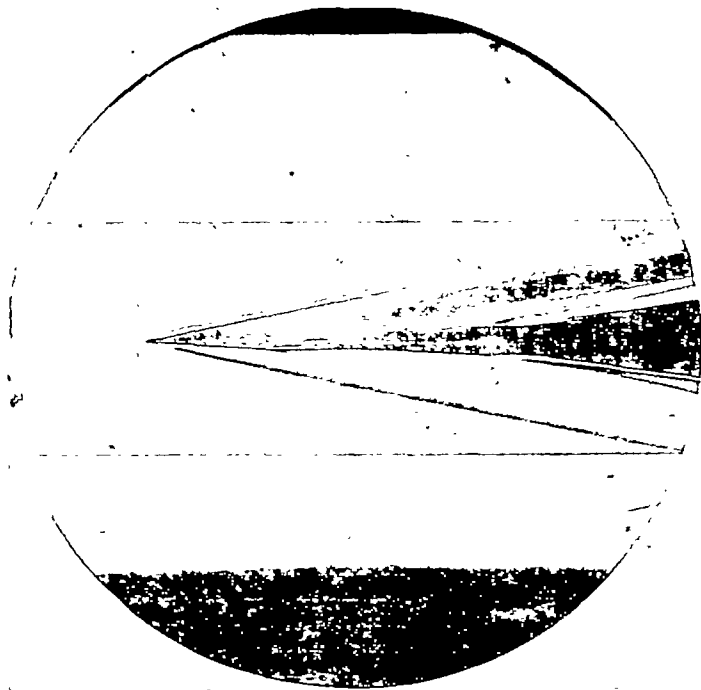


FIGURE 21.—Variation of center of pressure and lift-drag ratio with angle of attack for a 5-percent-thick half-circular-arc-section airfoil.  $M=6.86$ ;  $R=0.98 \times 10^6$ .

the spanwise variation of base pressure appeared to be within the scatter of the data. The ratio  $(p_b - p_\infty)/p_\infty$  varied from -0.47 at  $\alpha=0$  to about -0.55 at  $\alpha=\pm 10^\circ$ . A value of -0.50 appears to be representative for  $(p_b - p_\infty)/p_\infty$  over the whole range.

#### WING CHARACTERISTICS

Lift.—The lift coefficients obtained from experimental pressure and force data agree reasonably well although the values based on force data are slightly below those based on pressure measurements. (See figs. 14, 16, 18, and 20.) This decrement is ascribed to viscous and tip effects. There is no available theoretical method for rigorous calculation of the characteristics of complete wings. However, it may be possible to use the linearized theory to obtain an approximate



(a)  $\alpha = 0.5^\circ$

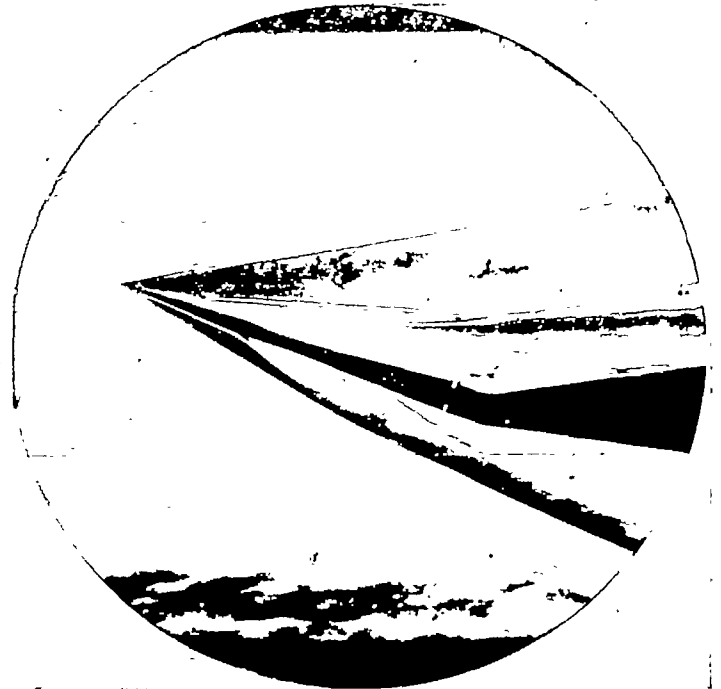


(b)  $\alpha = 7^\circ$

L-69126



(c)  $\alpha = 16.8^\circ$



(d)  $\alpha = 21.5^\circ$

L-69127

FIGURE 22.—Schlieren photograph of flow about a wing with a 5-percent-thick diamond section.



evaluation of the tip effects. The linearized theory predicts that tip effects will cause a reduction of about 7 percent in the initial lift-curve slope. An analysis of the pressure data indicates that viscous effects reduce the section lift-curve slope by about 12 percent at low angles of attack. The effect is decreased at high angles of attack so that the reduction in  $C_L$  due to these viscous effects (mainly separation) is only about 4 percent. Thus an average total reduction of about 15 percent from the value given by inviscid theory is indicated in the lift-curve slope; however, the force data for the diamond wing are only about 10 percent below the values given by inviscid theory, an indication that the tip effect is overestimated by the linearized theory. In general, the other airfoils show this same effect and the tip effects appear to cause only a 2- to 6-percent reduction in lift. Further investigation is required to evaluate the tip effect more accurately.

At moderate angles of attack, the flow separates at about the maximum thickness of the wing with the diamond section, as shown in the schlieren photograph (fig. 22 (c)). Similar separation occurs on the other wings. At these moderate angles of attack, the lift contribution of the upper surfaces is about 60 percent of the theoretical. At higher angles of attack, the flow separates farther forward on the upper surface and decreases the lift slightly. Complete loss of lift on the upper surface, however, does not occur for the wings having the diamond, half-diamond, and circular-arc airfoil sections. The schlieren photograph presented in figure 22 (d) shows that the separation does not occur immediately behind the leading edge. As a result, the pressures on the upper surface remain well below the free-stream pressure. Complete separation from the upper surface was observed for the wing with the wedge airfoil section at an angle of attack of  $20^\circ$  (though complete separation was not noted on the other wings even when the angle of attack of the upper surface was greater than that of wedge airfoil).

**Drag.**—At very low angles of attack, the drag coefficients from the pressure measurements were in good agreement with the values predicted by the inviscid-flow theory. (See figs. 14, 16, 18, and 20.) The drag coefficients from the force measurements at these low angles, however, were appreciably greater than those obtained from the pressure data. This increase in drag is primarily due to skin friction since the pressure effects due to the boundary layer on the various parts of the wings tend to compensate each other. The addition of the calculated friction-drag coefficient (see "Presentation of Results") to the results obtained from inviscid-flow theory resulted in theoretical values which were in good agreement with the experimental values. As the angle of attack was increased, however, the experimental drag coefficients tended toward slightly lower values than

predicted by theory because of the loss in lift from the upper surface and tip effects.

**Lift-drag ratios.**—The lift-drag ratios computed from both force and pressure data agree with the theoretical lift-drag ratios at high angles of attack (figs. 15, 17, 19, and 21). At low angles of attack, however, the experimental lift-drag ratios obtained from pressure data agree reasonably well with the inviscid theory. The force data agree with the theory when friction is considered, although considerable scatter in the force data is evident at low angles of attack. This scatter is due largely to the fact that the forces at the low angles of attack are very small and decrease the percentage accuracy of the force balance; however, the low-angle force measurements are of sufficient accuracy to indicate that the friction coefficients are of the correct magnitude.

The values of maximum lift-drag ratio vary considerably with wing airfoil section when obtained from pressure data but are practically constant when computed from force data. The maximum lift-drag ratios obtained from pressure data for the wings are summarized in the following table:

Fig.	Airfoil	Approximate $(L/D)_{max}$ from pressure data	Value of $\alpha$ for $(L/D)_{max}$
15	Diamond.....	$10\frac{1}{2}$	$3^\circ$
17	Half-diamond.....	$8\frac{1}{2}$	$4.5^\circ$
19	Wedge.....	10	$3^\circ$
21	Half-circular arc....	$7\frac{1}{2}$	$5.5^\circ$

Considerable scatter existed in the force data results; however, these results indicated that the maximum value of  $L/D$  was about 6 for all four airfoils.

In figure 19, for the wedge airfoil the theoretical inviscid lift-drag ratios have been included for base pressures equal to free-stream pressure, one-half of free-stream pressure, and zero absolute pressure. A base pressure of 50 percent of stream pressure was indicated in the base-pressure measurements (fig. 13). Good agreement is obtained between the wedge-airfoil force measurements and the theory that includes skin friction, when a base pressure of 50 percent of stream pressure is assumed.

The maximum lift-drag ratio for the half-circular-arc airfoil was lower than for the other airfoils; however, the angle of attack at which the maximum lift-drag ratio occurred was slightly higher than those for the other airfoils, so that at angles of attack above those required for peak  $L/D$  the lift-drag ratios were only slightly different. At lower angles of attack, however, considerably lower lift-drag ratios were obtained for the half-circular-arc airfoil.

**Center of pressure.**—In all cases, good agreement was obtained between experiment and theory for the centers of pressure (figs. 15, 17, 19, and 21). The locations of the center of pressure on the diamond airfoil sections varied from 40 percent to 45 percent of the chord (fig. 15). The wedge airfoil, as was to be expected, had a center of pressure at 50 percent of the chord over the whole range of angles of attack tested (fig. 19). For the wings with the half-diamond section and the half-circular-arc section the center of pressure moved rapidly away from the midchord position as the angle of zero lift was approached (figs. 17 and 21).

#### WING COMPARISONS

The inviscid theory and the results of pressure measurements indicate that the wings with the diamond and the wedge airfoils are considerably better than those with the half-diamond and the half-circular-arc airfoils when  $(L/D)_{max}$  is considered; however, when viscous effects are included, the differences in  $(L/D)_{max}$  are small and the choice of airfoil would probably be based on other considerations for the Reynolds number of this investigation. The minimum drag of the wings with the diamond and the wedge airfoils is slightly less than that of the wings with the other two sections, but the drag of the former two wings increases much more rapidly with angle of attack. Since the minimum drag of the wings is largely composed of skin friction, only moderate percentage reductions in total drag could be obtained by reducing the thickness below 5 percent at the test Reynolds number.

#### CONCLUSIONS

The results of tests of four wings of square plan form and 5-percent-thick diamond, half-diamond, wedge, and

half-circular-arc airfoil sections in the Langley 11-inch hypersonic tunnel at a Mach number of about 6.86 and Reynolds number of  $0.98 \times 10^6$  lead to the following conclusions:

1. Aerodynamic characteristics due to the pressure forces can be predicted with reasonable accuracy from two-dimensional inviscid theory for wings of square plan form at a Mach number of 6.86. At high angles of attack, the experimental values were, however, slightly lower than the values given by the inviscid theory because of separation and tip effects, and at low angles of attack, the skin friction should be taken into account in calculating the total drag coefficients and lift-drag ratios of wings.

2. The two wings with symmetrical airfoil sections (the diamond and wedge sections) had the highest maximum lift-drag ratios from pressure measurements and the wing with half-circular-arc sections had the lowest. The differences, however, were small when viscous effects were included, the overall maximum lift-drag ratio being close to 6 for all the wings tested.

3. Large deviations of the pressures from those predicted from inviscid theory existed at the leading edge of the wing and just behind sudden changes in surface slope because of a rapid growth of the laminar boundary layer at the high test Mach number.

4. The effect of boundary layer on the pressures on a flat surface parallel to the stream was in good agreement with theoretical results in which the boundary layer was assumed to be laminar.

LANGLEY AERONAUTICAL LABORATORY,  
 NATIONAL ADVISORY COMMITTEE FOR AERONAUTICS,  
 LANGLEY FIELD, VA., April 17, 1951.

#### REFERENCES

1. McLellan, Charles H., Williams, Thomas W., and Bertram, Mitchel H.: Investigation of a Two-Step Nozzle in the Langley 11-Inch Hypersonic Tunnel. NACA TN 2171, 1950.
2. McLellan, Charles H., Williams, Thomas W., and Beckwith, Ivan E.: Investigation of the Flow Through a Single-Stage Two-Dimensional Nozzle in the Langley 11-Inch Hypersonic Tunnel. NACA TN 2223, 1950.
3. Busemann, A.: Gasströmung mit laminarer Grenzschicht entlang einer Platte. Z.f.a.M.M., Bd. 15, Heft 1/2, Feb. 1935, pp. 23-25.
4. Von Kármán, Th., and Tsien, H. S.: Boundary Layer in Compressible Fluids. Jour. Aero. Sci., vol. 5, no. 6, Apr. 1938, pp. 227-232.
5. Bertram, Mitchel H.: An Approximate Method for Determining the Displacement Effects and Viscous Drag of Laminar Boundary Layers in Two-Dimensional Hypersonic Flow. NACA TN 2773, 1952.
6. Bertram, Mitchel H.: Viscous and Leading-Edge Thickness Effects on the Pressures on the Surface of a Flat Plate in Hypersonic Flow. Jour. Aero. Sci. (Readers' Forum), vol. 21, no. 6, June 1954, pp. 430-431.